Comparison between the classical theory predictions and molecular simulation results for heterogeneous nucleation of argon

Antti Lauri,[a] Evgeni Zapadinsky, Hanna Vehkamäki, and Markku Kulmala
Department of Physical Sciences, University of Helsinki, P.O. Box 64, FI-00014 University of Helsinki, Finland

(Received 28 April 2006; accepted 6 September 2006; published online 26 October 2006)

We have performed Monte Carlo simulations of homogeneous and heterogeneous nucleations of Lennard-Jones argon clusters. The simulation results were interpreted using the major concept posing a difference between the homogeneous and heterogeneous classical nucleation theories—the contact parameter. Our results show that the multiplication concept of the classical heterogeneous nucleation theory describes the cluster-substrate interaction surprisingly well even for small molecular clusters. However, in the case of argon nucleating on a rigid monolayer of fcc(111) substrate at $T=60$ K, the argon-substrate atom interaction being approximately one-third as strong as the argon-argon interaction, the use of the classical theory concept results in an underestimation of the heterogeneous nucleation rate by two to three orders of magnitude even for large clusters. The main contribution to this discrepancy is induced by the failure of the classical theory of homogeneous nucleation to predict the energy involved in bringing one molecule from the vapor to the cluster for clusters containing less than approximately 15 molecules. © *2006 American Institute of Physics*. [DOI: 10.1063/1.2358343]

I. INTRODUCTION

Heterogeneous nucleation is a candidate for triggering atmospheric aerosol activation processes.[1] For practical atmospheric applications it is important to predict the heterogeneous nucleation rate theoretically.[2] Usually the predictions are made using the classical heterogeneous nucleation theory (CHNT).[3] It is based on the same principles as the classical homogeneous nucleation theory (CNT);[4–7] molecular clusters are treated as liquid droplets with bulk liquid values for density and surface tension. When the interaction of a droplet with a substrate surface is taken into account, only one macroscopic parameter, namely, the contact angle between the nucleating droplet and the surface, is needed. There has been an attempt to substitute the macroscopic contact angle with a microscopic fit.[8] In atmospheric sciences there exist a number of studies where CHNT has been applied.[9–20]

Besides the classical theory, there exist a number of other methods available for the calculation of the major quantities in nucleation, namely, nucleation rate and free energy of formation. These methods include density functional approaches and molecular dynamics (MD) simulations. The density functional approaches,[21–25] based on the capillarity theory,[26] enable the determination of the free energy of formation from approximate free energy functionals. Using MD simulations it is possible to study the dynamical behavior of nucleating supersaturated vapor.[27–33]

With the development of computers the statistical mechanics (molecular) approach[34] to nucleation has become possible. It allows one to calculate straightforwardly the nucleation rate for homogeneous nucleation with Monte Carlo (MC) simulations. However, the practical application of the molecular approach is limited because of the complex nature of the intermolecular interaction. Most of Monte Carlo simulations related to nucleation are performed for argon[35–41] because of the simplicity of the intermolecular potential. On the other hand, experiment on the nucleation of argon is rather difficult,[42–48] and comparison of the theory and experiment does not allow conclusions on the validity of various nucleation theories. A recent experimental study by Fladerer and Strey,[49] suggesting a vast 30 orders of magnitude difference between experimental and theoretical nucleation rates, gives an extensive data set for future comparison. Aside from argon, experiments for homogeneous nucleation of water give more data for analysis. Neither CNT nor simulation results agree well with experimental values of nucleation rate, but the MC simulations reproduce the experimental temperature dependence while CNT fails to do so.[50–52]

Heterogeneous nucleation has not been studied as extensively as homogeneous nucleation using Monte Carlo techniques. There exist, however, some reports on molecular MC simulations of heterogeneous nucleation. The majority of the studies dealing with vapor-liquid or ice nucleation investigate either Lennard-Jones[53–56] or water[57–60] clusters interacting with a variety of substrate surfaces. The scope of these studies has been mainly to investigate either the structure of the cluster or the effect of the substrate structure on the free energy.

Recently, we have developed a molecular approach to heterogeneous nucleation.[61] Special attention was paid to peculiarities in the usage of the Monte Carlo simulations for studying heterogeneous nucleation. In the present study we utilize our simulation approach and compare the results to the classical heterogeneous nucleation theory concept of the

[a]Electronic mail: antti.lauri@helsinki.fi

multiplication of the homogeneous nucleation barrier height by the contact parameter. The simulated model system is an argon cluster on platinum substrate. Our main question is whether it is enough to know just the contact angle between the cluster and the substrate and the homogeneous nucleation rate in order to calculate the heterogeneous nucleation rate.

II. THE ENERGY BARRIER IN THE CLASSICAL NUCLEATION THEORY

In order to understand the features of the CHNT a brief presentation of the CNT is needed. Thus we first summarize the calculation of the formation free energy for homogeneous clusters.[62,63]

Consider a cluster consisting of n molecules suspended in supersaturated vapor where the temperature is T and the vapor pressure is p_g. The cluster is treated as an incompressible, uniform spherical liquid droplet of radius r, area $A=4\pi r^2$, and volume $\mathcal{V}_{\mathrm{hom}}=4/3\pi r^3$. Let ρ_l be the number density in the liquid. The total number of molecules in a cluster is then $n=\rho_l \mathcal{V}_{\mathrm{hom}}$. The free energy of formation in homogeneous nucleation for a one-component cluster is given by

$$\Delta G_{\mathrm{hom}} = A\sigma_{lg} - \rho_l \mathcal{V}_{\mathrm{hom}} kT \ln S, \tag{1}$$

where σ_{lg} is the vapor-liquid surface tension, k is the Boltzmann constant, and $S=p_g/p_s$ is the saturation ratio, where p_s is the saturation vapor pressure. Definition of the critical radius r^* as the maximum point of the formation free energy $(\partial \Delta G^*_{\mathrm{hom}}/\partial r^*=0)$ leads to

$$r^* = \frac{2\sigma_{lg}}{\rho_l kT \ln S}. \tag{2}$$

In heterogeneous nucleation the shape and nature of the substrate surface play an important role. In this study we concentrate on the most simple shape of the substrate—a flat, insoluble surface. Consider a critical embryo formed from the vapor phase on the surface. As in the homogeneous case, the cluster is thought to consist of incompressible, uniform liquid. The shape of the cluster is a segment of a sphere with the base attached to the insoluble surface. The angle θ between the embryo surface and the substrate surface is called the contact angle. A schematic picture in the upper part of Fig. 1 shows the geometry of the system. Now the volume $(\mathcal{V}_{\mathrm{het}})$, base area (A_{sl}), and cap area (A_{lg}) of the embryo can be expressed as functions of the embryo radius and contact angle as

$$\mathcal{V}_{\mathrm{het}} = \frac{\pi}{3} r^3 (2+\cos\theta)(1-\cos\theta)^2, \tag{3}$$

$$A_{lg} = 2\pi r^2 (1-\cos\theta), \tag{4}$$

$$A_{sl} = \pi r^2 (1-\cos^2\theta). \tag{5}$$

The ratio of the volumes of the droplet on the substrate and a spherical droplet is

$$\frac{\mathcal{V}_{\mathrm{het}}}{\mathcal{V}_{\mathrm{hom}}} = f(m) = \frac{n_{\mathrm{het}}}{n_{\mathrm{hom}}}, \tag{6}$$

where $f(m)=(2+m)(1-m)^2/4$ is called the contact parameter and $m=\cos\theta$.

In the classical theory the energy barrier for heterogeneous nucleation is given by[62]

$$\Delta G_{\mathrm{het}} = \rho_l(\mu_l - \mu_v)\mathcal{V}_{\mathrm{het}} + \sigma_{lg}A_{lg} + (\sigma_{sl}-\sigma_{sg})A_{sl}, \tag{7}$$

where μ is the chemical potential, σ is the interfacial free energy per unit area, $\mathcal{V}_{\mathrm{het}}$ is the volume of the cluster, and A is the surface area of the cluster. Subscripts l, g, and s correspond to the liquid and vapor phases and the substrate surface, respectively.

Inserting Eqs. (3)–(5) for volume and areas into Eqs. (1) and (7) we get

$$\Delta G_{\mathrm{het}} = \Delta G_{\mathrm{hom}} f(m). \tag{8}$$

Thus, according to the classical nucleation theory the free energies of formation in homogeneous and heterogeneous nucleations differ by the factor of the contact parameter. The critical radius in heterogeneous nucleation is exactly the same as in homogeneous nucleation. It should be noted that the contact parameter $f(m)$ is the same for the volume and energy barrier [Eqs. (6) and (8)] only if the substrate is planar.[20]

In order to find the difference between the work of formation of an n cluster and that of an $(n-1)$ cluster we will need to express the work of formation in terms of the number of molecules n. Using $\mathcal{V}_{\mathrm{hom}}=n/\rho_l$ we get

$$\Delta G_{\mathrm{hom}}(n) = -nkT\ln S + \beta n^{2/3}, \tag{9}$$

where $\beta=(36\pi)^{1/3}\rho_l^{-2/3}\sigma_{lg}$. Differentiating the work of

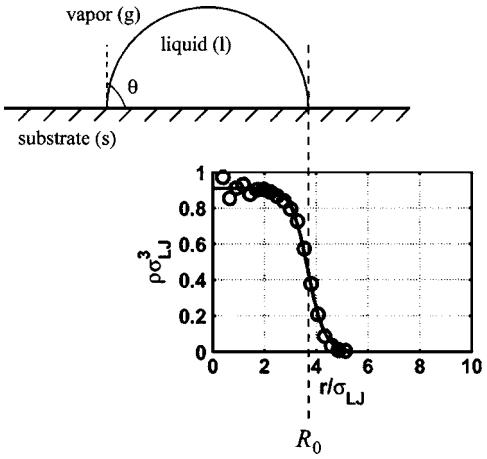

FIG. 1. A schematic picture of the geometry of a liquid embryo on a flat solid substrate. The angle θ is the contact angle. The picture also shows the connection between the classical droplet model and the equimolar radius obtained from the density distribution of the cluster.

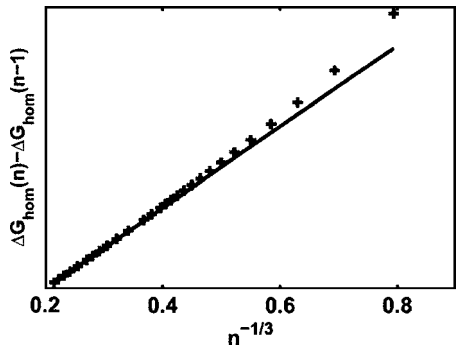

FIG. 2. An illustration of the derivative of the work of formation with respect to the number of molecules in the cluster (solid line) and the work of formation increment, i.e., the work to bring one molecule from the vapor to the cluster (crosses) for an arbitrary slope s_{hom}.

formation over the number of molecules we get

$$\frac{\partial \Delta G_{hom}(n)}{\partial n} = -kT \ln S + \frac{2}{3}\beta n^{-1/3}. \tag{10}$$

The approximated difference between the work of formation of an n cluster and that of an $(n-1)$ cluster is now given by

$$\Delta G_{hom}(n) - \Delta G_{hom}(n-1) \approx \frac{\partial \Delta G_{hom}}{\partial n}\Delta n, \tag{11}$$

where $\Delta n=1$. However, instead of using the derivative we should define the work of bringing one molecule from the vapor to the cluster. For this purpose we use the increment of the work of formation, given by

$$\Delta G_{hom}(n) - \Delta G_{hom}(n-1) = \tfrac{3}{2}s_{hom}[n^{2/3} - (n-1)^{2/3}] \quad (n \geqslant 2), \tag{12}$$

where s_{hom} is the slope of the (linear) derivative function. Figure 2 demonstrates the difference between the derivative of the work of formation with respect to the number of molecules in the cluster and the increment for an arbitrary slope s_{hom}. As it can be seen, Eq. (11) represents a good approximation for large clusters, but for small clusters there is a slight deviation between the derivative and the increment. In the data analysis of this study we have ignored this difference.

Using Young's equation

$$\sigma_{lg} m = \sigma_{sg} - \sigma_{sl}, \tag{13}$$

$\mathcal{V}_{het}=n/\rho_l=4/3\pi r^3 f(m)$, and Eqs. (4), (5), and (7) the difference between the work of formation of an n cluster in heterogeneous nucleation and that in homogeneous nucleation becomes

$$\Delta G_{het}(n) - \Delta G_{hom}(n) = \beta(f^{1/3}(m) - 1)n^{2/3}. \tag{14}$$

III. THE THEORY BEHIND THE SIMULATION METHOD

In this section we will summarize our molecular approaches for both homogeneous and heterogeneous nucleations.

A. Homogeneous nucleation

The most frequently used model for the imperfect gas considers the gas as a mixture of ideal gases, each of them representing clusters of a certain size. The clusters are assumed to be noninteracting with the monomers and with each other. For some simple pair potentials the equilibrium cluster distribution can be found analytically, while for the vast majority of cases computer simulations, especially Monte Carlo simulations, are used. There are different Monte Carlo approaches to the simulation of vapor nucleation. They can be divided into two categories. The first one is a direct simulation of vapor to observe clustering.[36,38,41] The second type is the simulation of an isolated cluster to calculate the cluster free energy,[34,39,51,52,64,65] the method presented also here. The simulations of the second type correspond strictly to the imperfect gas model described above. At first sight the direct vapor simulation seems to be more rigorous than the simulation of an isolated cluster. However, all the cited methods of the first type assume the validity of the following equilibrium cluster distribution:[66–71]

$$\mathcal{N}_n = \mathcal{N}_1 \exp\left(-\frac{\Delta G_{hom}(n)}{kT}\right), \tag{15}$$

where $\mathcal{N}_n$ is the number of n clusters and $\Delta G_{hom}(n)$ is often referred to as the reversible work of formation of an n cluster. From statistical mechanics we know that if an equilibrium cluster distribution exists, then the cluster concentration can be calculated through the cluster partition function. It means that the only more general feature of the direct vapor simulation is that the cluster partition function in that case takes the cluster-monomer and cluster-cluster interactions into account. As shown by Oh and Zeng,[72] their contributions are negligibly small unless the saturation ratio is extremely high. Comparisons between the prediction of the nucleation rate by methods of different types have been done earlier.[72–74] At similar conditions different simulation methods give nearly identical results. Simulations of an isolated cluster are much less time consuming by two reasons. First, they do not need very large number of molecules in the simulated system. Second, more importantly, while simulating the isolated cluster one does not need to input the saturation ratio as a parameter. As we shall see later, the dependence of the work of formation on the saturation ratio is fully described by the term proportional to $(n-1)kT \ln S$. The latter fact makes our study much easier, since our main goal is to check the validity of the CHNT prediction of the work of cluster formation in the heterogeneous case. CHNT predicts that the work of formation can be obtained through the work of a cluster formation in the homogeneous case and the contact parameter obtained via macroscopic consideration, when the interaction of the cluster molecules between each other and with the substrate molecules is described by a pair potential.

In our molecular approach of homogeneous nucleation we follow the formulation of Hale,[39] Hale and DiMattio,[52] and Hale and Ward[64] with the specifications made by Lauri *et al.*[74] The same way as in the classical theory, the vapor is considered as a mixture of ideal gases, each gas consisting of

clusters of one size, i.e., monomers make up one gas, dimers another, etc. The starting point for the calculation of the work of formation is Eq. (15). The work of formation is given by

$$\Delta G_{\mathrm{hom}}(n) = -kT\left[\ln\left(\frac{q(n)}{n!}\right) - n\ln q(1) - (n-1)\ln \mathcal{N}_1\right], \tag{16}$$

where $q(n)$ is the configurational integral of the n cluster,

$$q(n) = \int_{\mathrm{cluster}} \cdots \int \exp\left(-\frac{U_n(\boldsymbol{R}_1, \ldots, \boldsymbol{R}_i, \ldots, \boldsymbol{R}_n)}{kT}\right) \times d\boldsymbol{R}_1 \cdots d\boldsymbol{R}_n. \tag{17}$$

In Eq. (17) $\boldsymbol{R}_i$ is the position vector of the ith molecule in the laboratory coordinates and U_n is the potential energy of the cluster.

The specific values of the configurational integral for many-body systems such as molecular clusters are practically impossible to evaluate analytically. However, there exist computational methods able to measure the ratio of configurational integrals of two systems related to each other. Multiplying $q(i)/q(i-1)$ over all cluster sizes up to n we get

$$q(n) = \frac{q(n)}{q(n-1)}\frac{q(n-1)}{q(n-2)}\cdots\frac{q(2)}{q(1)}q(1). \tag{18}$$

The logarithm of this product can be transformed to the form

$$\ln q(n) = \sum_{i=2}^{n} \ln\left(\frac{q(i)}{q(i-1)}\right) + \ln q(1). \tag{19}$$

Now the work of formation of an n cluster is given by

$$\Delta G_{\mathrm{hom}}(n) = kT\sum_{i=2}^{n}\left[-\ln\frac{q(i)}{q(i-1)V} + \ln i - \ln \mathcal{N}_1\right], \tag{20}$$

since $q(1)=V$, where V is the volume of the system.

From this point onwards, the denominator $q(i-1)V$ in the logarithm inside the summation in Eq. (20) is treated slightly differently from Hale and Ward, producing a disparity between the two approaches in the partition function of the cluster.

After the transformation from the laboratory coordinates $\boldsymbol{R}$ to the center of mass coordinates $\boldsymbol{R}'$ the expression of the configurational integral for the n cluster becomes

$$q(n) = n^3 q_{\mathrm{c.m.}(n)}(n)V, \tag{21}$$

where

$$q_{\mathrm{c.m.}(n)}(n) = \int_{n\ \mathrm{cluster}} \cdots \int \exp\left(-\frac{U_n(\boldsymbol{R}'_1, \ldots, \boldsymbol{R}'_{n-1})}{kT}\right) \times d\boldsymbol{R}'_1 \cdots d\boldsymbol{R}'_{n-1}. \tag{22}$$

The term n^3 is the Jacobian determinant of the coordinate transformation, and

$$\int d\boldsymbol{R}_{\mathrm{c.m.}} = V. \tag{23}$$

Similarly in the center of mass coordinates $\boldsymbol{R}''$ for an $(n-1)$ cluster

$$q(n-1) = (n-1)^3 q_{\mathrm{c.m.}(n-1)}(n-1)V, \tag{24}$$

where

$$q_{\mathrm{c.m.}(n-1)}(n-1) = \int_{(n-1)\ \mathrm{cluster}} \cdots \int \exp\left(-\frac{U_{n-1}(\boldsymbol{R}''_1, \ldots, \boldsymbol{R}''_{n-2})}{kT}\right) \times d\boldsymbol{R}''_1 \cdots d\boldsymbol{R}''_{n-2} \tag{25}$$

and

$$\int d\boldsymbol{R}'_{\mathrm{c.m.}} = V. \tag{26}$$

Let us consider two systems labeled A and B. System A consists of n molecules in a cluster. The center of mass of system A is fixed. System B is otherwise exactly the same as system A, but there is one free molecule, which does not interact with the other molecules in the cluster. With this definition, the configurational integral of system A is the same as the configurational integral of the n cluster in the center of mass coordinates:

$$q_A(n) = q_{\mathrm{c.m.}(n)}(n). \tag{27}$$

As we will describe later, our simulations produce the ratio of the configurational integrals of systems A and B, $q_A(n)/q_B(n)$. To get the relation between the configurational integral of system B, $q_B(n)$, and the configurational integral of the $(n-1)$ cluster in its center of mass coordinates needed in Eq. (20), we will consider the configurational integral in more detail. Deciding that the nth molecule in the n cluster is always the one not interacting with the other cluster molecules we can write the configurational integral for system B in the center of mass coordinates of the n cluster simply as

$$q_B(n) = \int_{n\ \mathrm{cluster}} \cdots \int \exp\left(-\frac{U_n(\boldsymbol{R}'_1, \ldots, \boldsymbol{R}'_{n-1})}{kT}\right) \times d\boldsymbol{R}'_1 \cdots d\boldsymbol{R}'_{n-1}, \tag{28}$$

where $\boldsymbol{R}'_i$ is the coordinate of molecule i in the center of mass coordinates of the n cluster. After the transformation to the center of mass coordinates of a system of $n-1$ interacting molecules $(\boldsymbol{R}'')$ the configurational integral becomes

$$q_B(n) = \int_{n\ \mathrm{cluster}} \cdots \int \exp\left(-\frac{U_n(\boldsymbol{R}''_1, \ldots, \boldsymbol{R}''_{n-2})}{kT}\right) \times d\boldsymbol{R}''_1 \cdots d\boldsymbol{R}''_{n-2} d\boldsymbol{R}'_{\mathrm{c.m.}}(n-1)^3. \tag{29}$$

The center of mass position is fixed according to the n cluster. Thus, in system B the center of mass position includes also the coordinates of the free molecule. Integration over the

center of mass of the $(n-1)$ cluster reflects the movement of the center of mass in system B.

Instead of integrating over the center of mass coordinate of the $(n-1)$ cluster $\boldsymbol{R}'_{\mathrm{c.m.}}$ we can integrate over the free molecule, since

$$\boldsymbol{R}''_n = -n\boldsymbol{R}'_{\mathrm{c.m.}} \Rightarrow d\boldsymbol{R}'_{\mathrm{c.m.}} = \frac{d\boldsymbol{R}''_n}{n^3}, \tag{30}$$

where $1/n^3$ is the Jacobian determinant of the transformation. The transformation leads to

$$q_B(n) = \int_{n\ \mathrm{cluster}} \cdots \int \exp\left(-\frac{U_n(\boldsymbol{R}''_1, \ldots, \boldsymbol{R}''_{n-2})}{kT}\right) \times d\boldsymbol{R}''_1 \cdots d\boldsymbol{R}''_{n-2} d\boldsymbol{R}''_n \frac{(n-1)^3}{n^3}. \tag{31}$$

Now we have to consider the boundary conditions of the cluster definition. Whereas the cluster of n molecules is forced to follow the cluster definition, the cluster of $n-1$ interacting molecules and one free molecule does not necessarily fulfill the conditions required by the cluster definition for the $(n-1)$ cluster. To overcome this we will formally split the configurational integral into two parts:

$$q_B(n) = \int_{(n-1)\ \mathrm{cluster}} \cdots \int \exp\left(-\frac{U_n(\boldsymbol{R}''_1, \ldots, \boldsymbol{R}''_{n-2})}{kT}\right) \times d\boldsymbol{R}''_1 \cdots d\boldsymbol{R}''_{n-2} d\boldsymbol{R}''_n \frac{(n-1)^3}{n^3} + \int_{\substack{n\ \mathrm{cluster} \\ \mathrm{not}(n-1)\ \mathrm{cluster}}} \cdots \int \exp\left(-\frac{U_n(\boldsymbol{R}''_1, \ldots, \boldsymbol{R}''_{n-2})}{kT}\right) \times d\boldsymbol{R}''_1 \cdots d\boldsymbol{R}''_{n-2} d\boldsymbol{R}''_n \frac{(n-1)^3}{n^3}. \tag{32}$$

The first integral in Eq. (32) includes only those configurations of the cluster where $n-1$ interacting molecules form an $(n-1)$ cluster and together with the free molecule form an n cluster. The second integral includes only configurations where n molecules belong to the same cluster, but $n-1$ interacting molecules cannot be considered as an $(n-1)$ cluster.

Furthermore, integration over the position of the nth molecule gives the volume available for the free molecule. Now we will mark the sum of the two integrals in Eq. (32) as

$$q_B(n) = (I_1 + I_2)\frac{(n-1)^3}{n^3} = I_1[1+\delta(n)]\frac{(n-1)^3}{n^3}, \tag{33}$$

where $\delta(n)$ accounts for the configurations in system B, which do not fulfill the conditions required by the cluster definition for the $(n-1)$ cluster.

Since $I_1 = \langle \mathcal{V}_{\mathrm{free}} \rangle q_{\mathrm{c.m.}(n-1)}(n-1)$, where $\langle \mathcal{V}_{\mathrm{free}} \rangle$ is the canonically averaged volume available for the free molecule, when it forms an n cluster together with a cluster of $n-1$ interacting molecules, we will end up at

$$q_B(n) = \frac{\langle \mathcal{V}_{\mathrm{free}} \rangle q_{\mathrm{c.m.}(n-1)}(n-1)(n-1)^3}{n^3}[1+\delta(n)]. \tag{34}$$

Using Eqs. (27) and (34) the ratio between the configurational integrals of clusters of sizes n and $n-1$ is

$$\frac{q_{\mathrm{c.m.}(n)}(n)}{q_{\mathrm{c.m.}(n-1)}(n-1)} = \frac{q_A(n)\langle \mathcal{V}_{\mathrm{free}} \rangle (n-1)^3[1+\delta(n)]}{q_B(n)n^3}. \tag{35}$$

Using the conventional relation between the Helmholtz free energy difference between two systems, $F_A(n) - F_B(n)$, and the configurational integral ratios of the same systems, $q_A(n)/q_B(n)$,

$$F_A(n) - F_B(n) = -kT \ln\left(\frac{q_A(n)}{q_B(n)}\right), \tag{36}$$

and inserting Eqs. (21), (24), and (35) into Eq. (20) we will end in the expression for the reversible work of formation of an n cluster,

$$\Delta G_{\mathrm{hom}}(n) = \sum_{i=2}^{n} \left(F_A(i) - F_B(i) - kT \ln[1+\delta(i)] + kT \ln \frac{i}{\rho_{sv}\langle \mathcal{V}_{\mathrm{free}}(i) \rangle} - kT \ln S \right), \tag{37}$$

where we have used the relation of the monomer density to that in the saturated vapor (ρ_{sv}),

$$\frac{\mathcal{N}_1}{V} = \rho_{sv} S. \tag{38}$$

B. Heterogeneous nucleation

Our recent formulation of the reversible work of formation in heterogeneous nucleation[61] also starts from the equilibrium cluster distribution, now in the presence of a substrate surface the cluster is interacting with. This equilibrium cluster distribution can be given in a similar form as in the homogeneous case [Eq. (15)],

$$\mathcal{N}_{na} = \mathcal{N}_{1a} \exp\left(-\frac{\Delta G_{\mathrm{het}}(n)}{kT}\right), \tag{39}$$

where index a indicates the presence of a substrate. This formulation corresponds to equilibrium cluster distribution in the classical approach.[75] A similar approach has been employed earlier by Ward *et al.* for water clusters on AgI substrate.[57] Our formulation enables us to evaluate the work of formation in the heterogeneous case by[61]

$$\Delta G_{\mathrm{het}}(n) = [F_{\mathrm{het}}(n) - F_{\mathrm{hom}}(n)] - [F_{\mathrm{het}}(1) - F_{\mathrm{hom}}(1)] + \Delta G_{\mathrm{hom}}(n), \tag{40}$$

where $F(n)$ is the Helmholtz free energy of an n cluster in a volume near the substrate surface, where the interaction between the cluster and the substrate is significant. We will describe the definition of this volume in the next section.

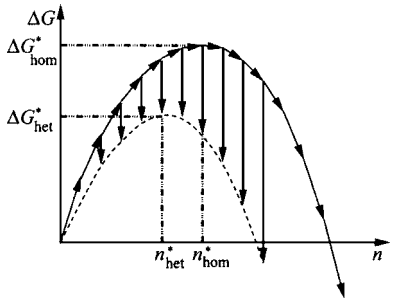

FIG. 3. A schematic picture of the procedure to obtain the complete energy barrier in homogeneous and heterogeneous nucleations. First each point in the energy barrier in homogeneous nucleation (upper curve with arrows) is calculated by the sum shown in Eq. (37), and each point in the heterogeneous nucleation barrier (dashed curve) is obtained by adding the Helmholtz free energy difference values (arrows pointing down) to the corresponding homogeneous nucleation barrier values according to Eq. (40). The critical cluster sizes and formation energies, corresponding to the maxima of the energy barriers, are denoted by n^* and ΔG^*, respectively.

IV. SIMULATION METHOD AND COMPUTATIONAL DETAILS

We applied the overlapping distribution method[76] in our simulations. This method provides an accurate way to determine the energy barriers in both homogeneous and heterogeneous nucleations. The general idea of this method is to compare two closely related systems by producing potential energy difference distributions. Simulation of each cluster size involves one separate simulation for both these systems.

All the interactions in our systems were described by the Lennard-Jones pair potential

$$\varphi_{ij}(R_{ij}) = 4\varepsilon\left[\left(\frac{\sigma_{\mathrm{LJ}}}{R_{ij}}\right)^{12} - \left(\frac{\sigma_{\mathrm{LJ}}}{R_{ij}}\right)^{6}\right], \tag{41}$$

where R_{ij} is the distance between molecules i and $j(i \neq j)$ and ε and σ_{LJ} are the energy and distance parameters of the selected potential, respectively. The values for the interaction between two cluster molecules were chosen to be $\varepsilon = 119.4$ K and $\sigma_{\mathrm{LJ}} = 3.4$ Å, whereas the values for the interaction between a cluster molecule and a substrate molecule were $\varepsilon = 43.8$ K and $\sigma_{\mathrm{LJ}} = 3.085$ Å, corresponding to argon-platinum interaction.[77] We carried out simulations with a truncated and shifted potential with a cutoff radius of $2.5\sigma_{\mathrm{LJ}}$.

The reversible work of formation of an n cluster in homogeneous nucleation is given by a sum of contributions over all cluster sizes smaller than n, as shown in Eq. (37). The work of formation in heterogeneous nucleation is obtained by adding four terms to the homogeneous work of formation [Eq. (40)]. This will allow us to determine the absolute values of formation energies for clusters on substrate surface and thus the energy barrier in heterogeneous nucleation by a chain of simulations. First we calculate the energy barrier up to n molecules in homogeneous nucleation and then add the four terms in each point of the barrier in order to get the barrier for heterogeneous nucleation. The schematic picture of the procedure is shown in Fig. 3.

In the simulation of homogeneous nucleation the two systems correspond to ensembles A and B described in Sec. III A. When simulating system A (cluster with n interacting molecules), the molecules in both systems were moved according to the Metropolis scheme[78] corresponding to the potential energy difference of system A. The potential energy difference between the systems was recorded in a probability distribution (histogram). Another probability distribution was generated during the simulation of system B (cluster with $n-1$ interacting molecules and one free molecule), where the acceptance of the Metropolis moves corresponded to the potential energy difference of system B. In both simulations of systems A and B the n-molecule center of mass position was kept fixed. The overlapping region of the two probability distributions gives the Helmholtz free energy difference between the two systems:

$$F_A(n) - F_B(n) = U_A(n) - U_B(n) + kT \ln\left(\frac{\mathcal{P}_A[U_A(n) - U_B(n)]}{\mathcal{P}_B[U_A(n) - U_B(n)]}\right), \tag{42}$$

where $U_A(n) - U_B(n)$ is the total potential energy difference between systems A and B.

Besides the Helmholtz free energy difference, Eq. (37) contains two unknown values. The term $\ln(1+\delta)$ includes the effect of the configurations breaking the cluster definition in system B. $\mathcal{V}_{\mathrm{free}}$ is the canonically averaged volume available for the free molecule, when it forms an n cluster together with a cluster of $n-1$ interacting molecules. The values of $\ln(1+\delta)$ and $\mathcal{V}_{\mathrm{free}}$ were obtained from the same simulations as the probability distributions. Their calculation depends on the cluster definition. In our simulations we used the cluster definition of Stillinger[79] with the connectivity distance of $1.5\sigma_{\mathrm{LJ}}$.

When using the Stillinger definition, the boundary condition discussed in the context of the second integral in Eq. (32) is constituted of such configurations where the free molecule in an n cluster forms the only link between two parts of the cluster. Thus, the exclusion of the free molecule would break the $(n-1)$ cluster in two parts. The idea of the overlapping distribution method can be used for the calculation of the term $\ln(1+\delta)$ as well. When simulating system B, the configurations where the free molecule is the only link between two parts of the cluster are not forbidden. Instead, we introduce system C, which is exactly the same as the system B, but where the configurations breaking the cluster definition in system B are either forbidden or have very high positive energy. Applying an "imaginary overlapping distribution method," the idea shown in Fig. 4, we are able to formulate the additional term. The ratio between the configurational integrals of the two systems (i.e., their free energy difference) is then obtained as the ratio $\mathcal{P}_C/\mathcal{P}_B$ at the only overlapping point $(\Delta U \equiv U_C - U_B = 0)$. By means of the term $1+\delta(n)$ in Eq. (33) this difference is now given by

$$1 + \delta(n) = \frac{N(n)}{N(n) - N_e(n)}, \tag{43}$$

where $N(n)$ is the total number of sampled configurations of an n cluster and $N_e(n)$ is the number of the configurations, in which the noninteracting molecule is the only link between two parts of the cluster. In practice N_e is calculated when simulating system B. Thus, there is no need to simulate system C separately.

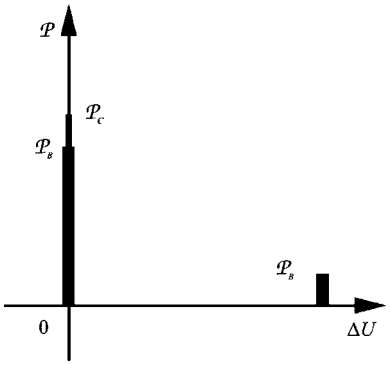

FIG. 4. A schematic picture of the idea of the "imaginary overlapping distribution method" to obtain a numerical value for the term $\ln(1+\delta)$ in Eq. (37). The bars indicate the number of configurations in ensembles B and C described in the text. The potential energy difference ΔU between ensembles B and C is different only for clusters breaking the cluster definition in ensemble B. Ensemble C is not simulated separately, but the number of configurations that break the cluster definition in ensemble B is recorded during the ensemble B simulation.

During the simulations a numerical value for the canonically averaged volume $\langle \mathcal{V}_{\text{free}} \rangle$ available for the free molecule was done by a set of simple brute force Monte Carlo runs. For each randomly chosen configuration we placed a sphere centered in the center of mass position of the $(n-1)$ cluster. The radius of the sphere was the connectivity distance of the cluster definition added to the distance between the center of mass and the molecule furthest from the center of mass. Evenly distributed random points inside this sphere were selected for the configuration during the simulation of ensemble A, and the number of points belonging to the cluster according to the cluster definition was counted. Then the available volume was obtained by multiplying the volume of the sphere and the fraction of the points belonging to the cluster. Averaging was done over 2000 configurations.

When simulating heterogeneous nucleation, the two simulated systems correspond to the ensemble which includes the cluster interacting with the substrate and the ensemble where the cluster does not interact with the substrate. The substrate was represented by a monolayer of rigid molecules set in the shape of a fcc(111) lattice. The nearest neighbor distance was set to 2.77 Å, representing the surface of a platinum crystal. The substrate size was 20×20 molecules. In order to represent a seemingly infinite substrate we restricted the center of mass position of the cluster to lie on the normal of the middle unit cell of the lattice. If the center of mass moved outside the middle unit cell boundaries, periodical boundary conditions were applied. Again, one probability distribution was produced from simulations of each ensemble, and Helmholtz free energy difference was obtained from the overlapping region of the probability distributions. The system where the cluster does not interact with the substrate is equivalent to system A. This information was utilized to calculate the explicit value of the work of formation in heterogeneous nucleation.

In both simulations of homogeneous and heterogeneous nucleations we used a factor λ to distinguish the two compared systems. In simulations of homogeneous clusters the factor λ was used to control the interaction between the free molecule and other cluster molecules. Value $\lambda=1$ corresponds to system A with n interacting molecules, while value $\lambda=0$ is equivalent to system B with $(n-1)$ interacting molecules and one free cluster molecule. Following the same idea, in heterogeneous cluster simulations value $\lambda=1$ corresponds to full interaction between the cluster and the substrate, while $\lambda=0$ implies that there is no interaction between the cluster and the substrate. In order to have a reasonable overlapping range of the probability distributions we performed the heterogeneous nucleation simulations in several stages, using intermediate values $\lambda=0.05$, $\lambda=0.2$, and $\lambda=0.5$.

Particularly when simulating ensembles where the cluster molecules do not interact either with the substrate or each other, i.e., using $\lambda=0$, very high potential energy differences between the systems arise due to molecules getting very near each other, weakening the ensemble average. To prevent this disturbance we restricted the nearest allowed distance between two molecules to the value of $0.83\sigma_{\text{LJ}}$, reasoned in our earlier work.[61]

A volume where the interaction between the cluster and the substrate is significant has to be defined for the heterogeneous nucleation simulations.[61] This volume is characterized by a limiting height h_{lim}. During the simulations the cluster molecules are not allowed to exceed this height. In our simulations we used the height where the potential energy between the cluster and the substrate equals 10^{-4} times the maximum mean interaction. In this study the value of this height varies between 7.5 Å for a monomer and 20.3 Å for a cluster of 195 molecules.

In order to equilibrate the systems we always generated $2n \times 10^5$ configurations, where n is the number of molecules in the cluster. We used further $n \times 10^6$ configurations to accumulate the histograms. During the equilibration we generated the subsequent configurations by performing translation trials, which were accepted following the Metropolis algorithm. In simulations of heterogeneous nucleation a full interaction between the cluster molecules and the substrate molecules was applied throughout the equilibration.

We made all the simulations in temperature $T=60$ K, which is above the triple point for the truncated and shifted potential we used.[80] It should be noted that often the liquid-vapor coexistence properties can be applied also below the triple point, since small nucleating clusters have been noticed to behave liquidlike even in very low temperatures (see, e.g., the work of Fladerer and Strey[49] and the references within).

V. RESULTS AND DISCUSSION

We carried out a series of Monte Carlo simulations. One set of simulations was run to obtain the work of formation in homogeneous nucleation for clusters of size of 2-900, and another one for calculating the difference between the work of formation of the clusters in homogeneous nucleation and that in heterogeneous nucleation for clusters of size of 1-195.

According to the classical theory heterogeneous nucleation is closely related to homogeneous nucleation; the contact parameter is the only quantity needed to obtain the work of the droplet formation in heterogeneous nucleation from

the work of formation in the homogeneous case. Next we specify some consequences of this theory. First, the classical nucleation theory is based on the assumption that the density of the droplets is identical for the same substance nucleating in homogeneous and heterogeneous conditions. Second, the ratio of the number of molecules in the critical cluster in the heterogeneous and homogeneous cases gives the contact parameter according to Eq. (6). Furthermore, the ratio of the critical work of formation in heterogeneous nucleation and in homogeneous nucleation also equals the contact parameter [Eq. (8)]. Thus, the curve of the work of formation versus the cluster size in the homogeneous case can be matched with the same curve in the heterogeneous case if the axes of the former curve are multiplied by the contact parameter. Third, the increment of the work of formation in the homogeneous case is given by Eq. (10). If $\partial \Delta G_{\mathrm{hom}}/\partial n$ is plotted versus $n^{-1/3}$, we obtain a straight line with a slope $s_{\mathrm{hom}}=\frac{2}{3}\beta$. According to Eq. (14) $\Delta G_{\mathrm{het}}(n)-\Delta G_{\mathrm{hom}}(n)$ also produces a straight line with a slope $s_{\mathrm{het}}=\beta[f^{1/3}(m)-1]$ if plotted versus $n^{2/3}$. The ratio of the slopes is thus

$$\frac{s_{\mathrm{het}}}{s_{\mathrm{hom}}}=\tfrac{3}{2}[f^{1/3}(m)-1]. \tag{44}$$

We performed simulations in order to check the validity of these classical relations. During the simulations we analyzed the shape and density of the clusters. The cluster densities were calculated using two different methods. The first way follows the proposal of Stillinger (1963).[79] In his paper he suggested that the volume of a cluster should be considered as the total volume occupied by spheres with radius given by half of the connectivity distance, which corresponds to $0.75\sigma_{\mathrm{LJ}}$ around each cluster molecule in our case. The second method, used only for homogeneous clusters, is based on a fit function of the form[81]

$$\rho(r)=\tfrac{1}{2}(\rho_l+\rho_g)-\tfrac{1}{2}(\rho_l-\rho_g)\tanh[2(r-R_0)/D], \tag{45}$$

where ρ_l and ρ_g correspond to liquid and vapor phase densities, respectively, R_0 is the equimolar radius, and D is the surface thickness. The equimolar radius corresponds to the radius of a spherical droplet with uniform density ρ_l. In the fit function ρ_l, R_0, and D were free parameters. The vapor density was set to zero, since we did not simulate the surrounding vapor. Equation (45) gives the droplet radial density, where $r=0$ is the center of the droplet. An example of a radial distribution is shown in the lower part of Fig. 1 with the equimolar radius R_0 related to the classical droplet model. In the case of the homogeneous cluster the center of the cluster was set to the center of mass. The densities calculated from the Stillinger volume of homogeneous and heterogeneous clusters and the bulk liquid value of the homogeneous cluster density in Eq. (45) are shown in Fig. 5.

From Fig. 5 we can see that the densities calculated according to the Stillinger volume are practically identical for homogeneous and heterogeneous cases. However, both are lower than the density of the bulk liquid calculated for the homogeneous clusters. Unfortunately we could not calculate the bulk density from the simulations of the heterogeneous clusters, because the shape of clusters is far from being symmetric due to the interaction with the substrate.

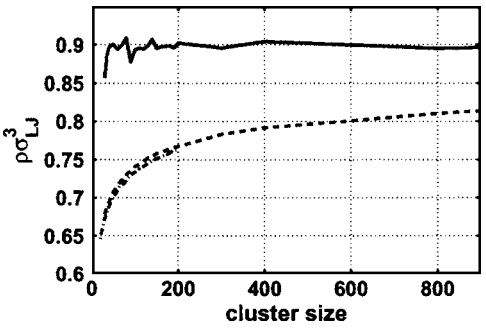

FIG. 5. Densities of the simulated clusters. The dashed curve represents the density of the Stillinger volume of the homogeneous cluster. The dash-dotted curve corresponds to the density of the heterogeneous cluster. The solid curve represents the bulk droplet density value ρ_l of the homogeneous cluster obtained from a fit of the form presented in Eq. (45).

To study the role of the contact parameter we first simulate homogeneous clusters. We calculate the work of formation using Eq. (37), where the term under the summation is the increment of the work of formation from an $(n-1)$ cluster to an n cluster,

$$\begin{aligned}\Delta G_{\mathrm{hom}}(n)-\Delta G_{\mathrm{hom}}(n-1)&=F_A(n)-F_B(n)-kT\ln[1+\delta(n)]\\&\quad+kT\ln\frac{n}{\rho_{sv}\langle \mathcal{V}_{\mathrm{free}}(n)\rangle}-kT\ln S.\end{aligned} \tag{46}$$

We observe that the only term independent of n in Eq. (46) $(-kT\ln S)$ is exactly the same as in the classical theory [Eq. (10)]. Therefore, if the classical homogeneous nucleation theory is valid, then the other terms altogether should have a linear dependence on $n^{-1/3}$. These terms correspond to the surface energy in the classical nucleation theory. Therefore we use the concept of surface energy difference between an n and an $(n-1)$ cluster, δf_{surf}:

$$\begin{aligned}\delta f_{\mathrm{surf}}(n)&\equiv F_A(n)-F_B(n)-kT\ln[1+\delta(n)]\\&\quad+kT\ln\frac{n}{\rho_{sv}\langle \mathcal{V}_{\mathrm{free}}(n)\rangle}\sim n^{-1/3}.\end{aligned} \tag{47}$$

As described in Sec. IV, we obtain the Helmholtz free energy difference $F_A(n)-F_B(n)$, the term $1+\delta(n)$, as well as the volume available for the free molecule $\mathcal{V}_{\mathrm{free}}(n)$ from our simulations. The only parameter remaining unknown in Eq. (47) is the saturated vapor density ρ_{sv}. Unfortunately there are no simulated saturated vapor pressures or densities at 60 K for the truncated and shifted Lennard-Jones potential. For higher temperatures simulations show that ρ_{sv} for the truncated and shifted potential is different from the full Lennard-Jones potential and from the experimental data for argon.[82] We chose the value of $\rho_{sv}(60\ \mathrm{K})=3.56\times10^{-4}\sigma_{\mathrm{LJ}}^{-3}$ in our simulations. This value was obtained using Wagner's approach[83] to calculate the saturated vapor pressure, when the pressure and temperature of the critical point are known:

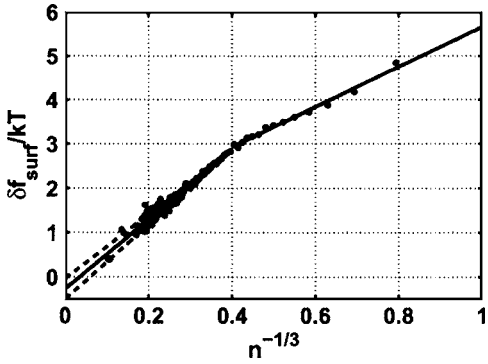

FIG. 6. The simulated surface energy difference δf_{surf} as a function of cluster size (shown as $n^{-1/3}$) in homogeneous nucleation calculations. The dots correspond to values obtained from single simulation runs and the solid line represents the two parts of the linear fit explained in the text. The dashed lines are the error lines for large clusters.

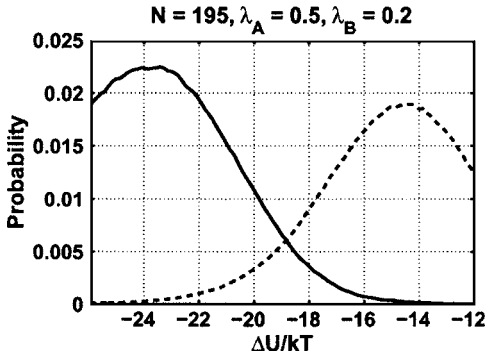

FIG. 7. An example of the histograms produced in the simulations comparing the formation free energy difference between homogeneous and heterogeneous nucleations. In this example the values of λ corresponding to the interaction strength between the cluster molecules and surface atoms are λ =0.5 and λ=0.2. The cluster consists of 195 argon molecules.

$$p_s = p_C \exp\left[\left(-5.904\,188\,529\left(1-\frac{T}{T_C}\right)\right.\right.$$
$$+1.125\,495\,907\left(1-\frac{T}{T_C}\right)^{1.5}$$
$$-0.763\,257\,912\,6\left(1-\frac{T}{T_C}\right)^{3}$$
$$\left.\left.-1.697\,334\,376\left(1-\frac{T}{T_C}\right)^{6}\right)\right], \tag{48}$$

where p_C and T_C are the critical pressure and temperature, respectively. We selected the values according to the truncated and shifted potential values $T_C^*=1.085$ and $p_C^*=0.0908$.[82]

In Fig. 6 we have plotted $\delta f_{\mathrm{surf}}(n)$ vs $n^{-1/3}$. Individual simulation results are shown by dots. As we can see, the surface energy difference does not follow a linear dependence throughout the whole cluster size range. Nevertheless, the differences can be approximated with two lines, one for small clusters ($n<16$) and another for larger clusters ($n \geqslant 16$). The slopes of the straight lines are $s_{\mathrm{hom}}^{\mathrm{large}}=(7.8\pm0.4)kT$ and $s_{\mathrm{hom}}^{\mathrm{small}}=4.6kT$ for large and small clusters, respectively. Earlier, Hale[39] has observed a similar behavior of the clusters of Lee *et al.*[34] As noted in Fig. 2 and the explanation within, a linear fit does not correspond exactly to the work of formation increment (i.e., surface energy difference) but to the derivative of the work of formation with respect to $n^{-1/3}$. A small deviation for the derivative of the surface term for small n is expected and is usually taken into account in modified liquid drop models.[84,85]

As expected, the extrapolated straight line in Fig. 6 goes to zero for infinitely large clusters ($n^{-1/3}=0$). According to the classical theory the surface energy difference between an n and an $(n-1)$ cluster must go to zero when the cluster size approaches infinity. It is natural to expect this also for the molecular theory, because very large (infinite) clusters should behave like bulk liquid.

The slopes representing larger clusters in Fig. 6 can be transformed into a numerical estimate of surface tension. As noted earlier, $s_{\mathrm{hom}}=\frac{2}{3}\beta$. Thus,

$$\sigma_{lg} = \rho_l^{2/3}\left(\frac{32}{3}\pi\right)^{-1/3} s_{\mathrm{hom}}. \tag{49}$$

Using the droplet bulk liquid density $\rho_l^* \approx 0.90$ (Fig. 5) we get $\sigma_{lg}=0.016\pm0.001$ N/m, which agrees well with the estimation produced by the equation presented by Sprow and Prausnitz,[86]

$$\sigma_{lg} = 0.037\,78\ \frac{\mathrm{N}}{\mathrm{m}}\left[1-\left(1-\frac{T}{T_C}\right)\right]^{1.277}, \tag{50}$$

giving surface tension $\sigma_{lg}=0.0168$ N/m at $T=60$ K, when $T_C^*=1.085$. The slope representing clusters smaller than 16 molecules in size is more problematic to turn into a specific value for surface tension, since the density inside the cluster becomes difficult to determine as practically all molecules are located on the surface of the cluster. Thus, we are not providing a numerical estimation for the surface tension of the smallest clusters.

Our heterogeneous nucleation simulation method[61] uses homogeneous nucleation as a reference point. Its outcome is the difference between the work of cluster formation in the heterogeneous case and that in the homogeneous case [Eq. (40)]. The simulations for each cluster size were run at four stages, varying the parameter λ describing the interaction strength between the cluster and the substrate. An example of a probability distribution pair is shown in Fig. 7. The Helmholtz free energy difference was calculated from the overlapping part of the histograms using Eq. (42).

We have plotted simulated values $\Delta G_{\mathrm{het}}(n)-\Delta G_{\mathrm{hom}}(n)$ vs $n^{2/3}$ in Fig. 8. It can be seen that the simulated data produce a straight line in these coordinates. Remembering that a small cluster might deviate from the classical model we have analyzed data also without clusters containing less than 16 atoms. Surprisingly, the slopes of the lines are almost identical with and without the 15 smallest clusters. The numerical value of the slope is $s_{\mathrm{het}}=-2.35kT$.

The slope of the formation energy difference s_{het} in Fig. 8 enables us to calculate the contact parameter $f(m)$, when the slope of the surface energy difference between an n and an $(n-1)$ cluster in homogeneous nucleation s_{hom} is known. Equation (44) is used for this purpose, yielding

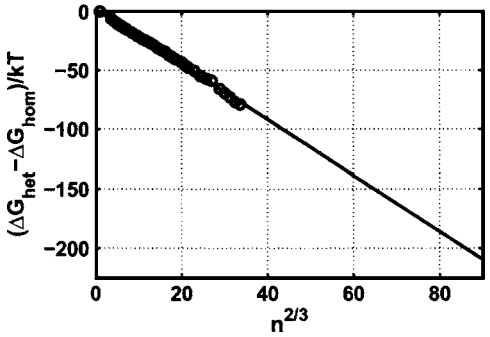

FIG. 8. The simulated difference $\Delta G_{\mathrm{het}}(n)-\Delta G_{\mathrm{hom}}(n)$ (circles) as a function of the cluster size and a linear fit of the difference on $n^{2/3}$ (solid line).

$$f(m)=\left(\frac{2}{3}\frac{s_{\mathrm{het}}}{s_{\mathrm{hom}}}+1\right)^3. \tag{51}$$

Unlike the estimate for the surface tension, the contact parameter can be well estimated for both small and large clusters: $f(m)=0.28$ $(n<16)$ and $f(m)=0.51\pm0.03$ $(n\geqslant 16)$.

We calculated the work of cluster formation in the homogeneous and heterogeneous cases using Eqs. (37) and (40), respectively. The size of the cluster that corresponds to the maximum of the curve of the work of formation is the critical cluster size. Work of formation curves for saturation ratios of 10 and 3 are presented in Figs. 9 and 10, respectively. The critical cluster size depends strongly on the saturation ratio in both heterogeneous and homogeneous cases. In $S=10$ the critical cluster sizes are $n^*_{\mathrm{hom}}=27$ and $n^*_{\mathrm{het}}=15$. In the lower saturation ratio $S=3$ the critical cluster sizes are naturally larger, $n^*_{\mathrm{hom}}=184$ and $n^*_{\mathrm{het}}=94$.

We multiplied the axes of the homogeneous formation free energies in different saturation ratios by the ratio of the simulated critical cluster sizes in heterogeneous and homogeneous nucleations. According to CHNT this ratio equals the contact parameter [Eq. (8)]. For high saturation ratios, when the critical clusters are rather small, the mismatch of the simulated and multiplied curves is clearly visible (see Fig. 9). For lower saturation ratios, when critical clusters are rather large, the relative mismatch of the curves is much smaller (see Fig. 10).

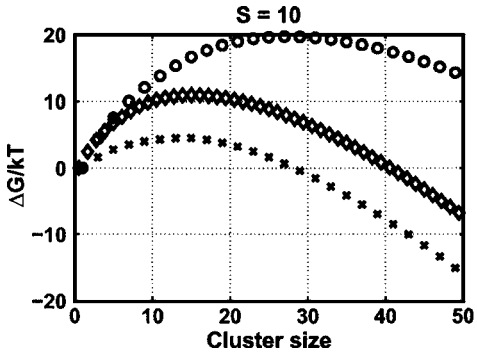

FIG. 9. Work of formation as a function of cluster size for both homogeneous and heterogeneous nucleations. The simulated energy barrier of homogeneous nucleation is denoted by circles, whereas the crosses represent the simulated heterogeneous nucleation energy barrier. The points marked by diamonds represent the heterogeneous nucleation formation energy obtained by multiplying both axes of the homogeneous nucleation barrier by the contact parameter $f(m)$. $S=10$.

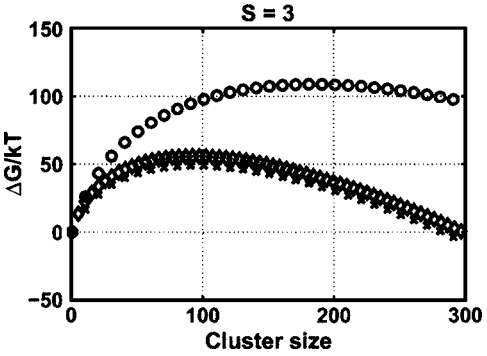

FIG. 10. Same as Fig. 9, but for $S=3$.

At first sight it seems that the $f(m)$ multiplication concept of the classical heterogeneous theory is erroneous only for small clusters, but works well for large clusters. However, even for large clusters there is a difference between the simulated heterogeneous critical work of formation value and the one obtained by multiplying the homogeneous critical formation energy by the contact parameter obtained as the ratio of the critical cluster sizes. This difference defines the ratio of the simulated heterogeneous nucleation rate and the rate predicted from the homogeneous nucleation rate and the value of the contact parameter. We have plotted this ratio versus critical cluster size in Fig. 11. We calculated the energy barrier in homogeneous nucleation using the formation energy increment corresponding to both two slopes in Fig. 6: the steeper slope for large clusters $(n>15)$ and the gentle slope for clusters smaller than or equal to 15 molecules in size. Two curves for the free energy of formation in heterogeneous nucleation were then obtained from the simulation results: one using Eq. (40) and the other by multiplying the homogeneous formation energy curves by the contact parameter. The ratio of the critical formation energies in heterogeneous nucleation is shown in Fig. 11. As expected, the ratio approaches unity when the critical cluster size increases. However, for the smallest clusters the critical formation energy obtained by multiplying the homogeneous cluster formation energy by the contact parameter is almost eight times the energy obtained from the simulations.

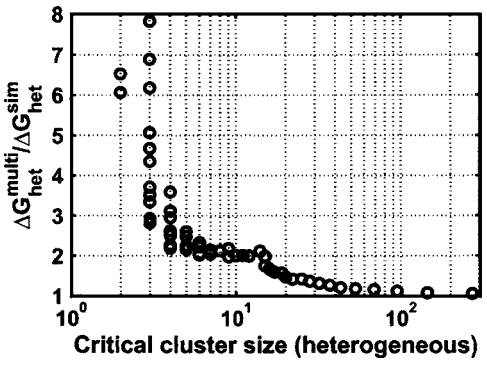

FIG. 11. Ratio of the critical formation energies obtained by the multiplication procedure and the simulations.

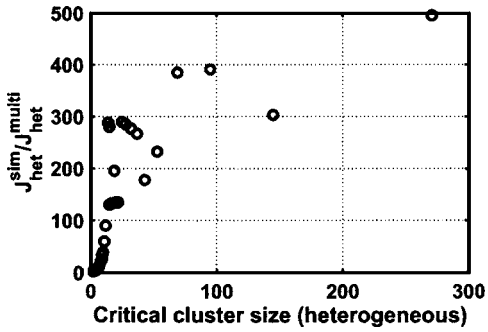

FIG. 12. Ratio of the heterogeneous nucleation rates calculated using Eq. (52).

The ratio of the nucleation rates given by the simulations ($J_{\mathrm{het}}^{\mathrm{sim}}$) and by the homogeneous nucleation energy barrier multiplied by the contact parameter ($J_{\mathrm{het}}^{\mathrm{multi}}$) is given by

$$\frac{J_{\mathrm{het}}^{\mathrm{sim}}}{J_{\mathrm{het}}^{\mathrm{multi}}} = \exp\left(\frac{\Delta G_{\mathrm{het}}^{\mathrm{multi}*} - \Delta G_{\mathrm{het}}^{\mathrm{sim}*}}{kT}\right). \tag{52}$$

This ratio is shown as a function of the critical cluster size in Fig. 12. We note that the nucleation rate calculated from the work of formation obtained by the multiplication results in an underestimation of the simulated nucleation rate. For small clusters the difference is approximately two orders of magnitude. However, the discrepancy does not decrease when the critical cluster size increases. In fact, the ratio of the nucleation rates even shows an increasing trend for larger critical cluster sizes, approaching three orders of magnitude for the largest clusters under investigation.

According to the classical theory the contact parameter $f(m)$ is the same for all critical cluster sizes (and thus different saturation ratios), as demonstrated by Eqs. (3)–(8). We calculated the simulated contact parameter using the ratio of the critical cluster sizes in the heterogeneous and homogeneous cases. As Fig. 13 shows, the contact parameter is fairly constant for critical cluster sizes larger than 20. However, for decreasing critical cluster sizes there is a clear decreasing trend of the contact parameter. This discrepancy with the CHNT is not surprising, since the classical theory assumes the same structure for critical clusters of all sizes. This assumption is not made in the simulations.

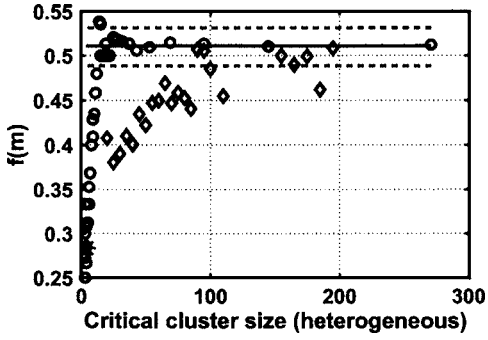

FIG. 13. The contact parameter obtained from the ratio of the critical cluster sizes of heterogeneous and homogeneous nucleations [Eq. (6)]. The parameters based on the two different slopes in Fig. 6 are shown by circles, and the diamonds represent the contact parameters calculated from the visually analyzed contact angle. The contact parameters obtained by Eq. (51) from the slopes in Figs. 6 and 8 are shown by the star for the small clusters ($n<16$) and the solid line for the large clusters ($n\geqslant 16$) along with the error lines denoted by the dashed line.

The contact angle can be obtained also via visual analysis. This was done by placing a circle going through three points: the two molecules of the cluster lying furthest from each other and the one having the furthest distance from the substrate surface level. The center of the circle then defined the center of a sphere having the same radius as the circle, confining practically all the cluster molecules. Using Eq. (45) we can determine surface thickness D, which defines the radius range where the cluster density decreases from the bulk value to zero. By subtracting $D/2$ from the radius of the confining sphere we get the equimolar radius. The contact angle was then defined as the angle between the plane $0.83\sigma_{\mathrm{LJ}}$ over the substrate surface plane and the surface of the sphere having the equimolar radius. The distance corresponds to the nearest allowed distance between a cluster molecule and a substrate atom. The description above is in agreement with the classical droplet model. The contact parameter values corresponding to the visual contact angles are shown as diamonds in Fig. 13. The visual values approach the contact angle obtained from the ratio of the critical cluster sizes, but only reach these values at cluster size around 100. In despite of this, the contact parameter obtained from the ratio of the simulated critical free energies in heterogeneous and homogeneous nucleations can be successfully used for critical clusters well below 100 in size.

VI. CONCLUSIONS

In this study we have used the molecular approach to heterogeneous nucleation in Monte Carlo simulations in order to see the performance of the $f(m)$ multiplication concept of the classical theory of heterogeneous nucleation. We studied Lennard-Jones argon nucleating on a monolayer of platinum ordered in the shape of a fcc(111) lattice.

Our results show that the classical nucleation theory multiplication concept is able to describe the cluster interaction with the substrate surprisingly well, even for small molecular clusters. However, calculation of the heterogeneous nucleation rate using the homogeneous nucleation rate and the contact parameter as the starting points gives a two to three orders of magnitude underestimation of the nucleation rate in our system at $T=60$ K. The major part of this difference arises from the failure of the classical theory of homogeneous nucleation to correctly reproduce the behavior of the free energy in bringing one of the vapor molecules into the cluster for clusters smaller than about 15 molecules. The difference is, however, not present only on high vapor supersaturations, when the critical cluster size is small. Quite the contrary, the underestimation gets even worse when the saturation ratio is decreased.

Supposing that there exist experimental data for the homogeneous nucleation rate and contact angle, the heterogeneous nucleation rate can be estimated by two to three orders of magnitude accuracy according to our results. The accuracy is, however, expected to be different for other substances as well as other pair potential interaction parameters.

ACKNOWLEDGMENT

One of the authors (A.L.) would like to thank J. Merikanto for fruitful discussions.

[1] M. Kulmala, K. E. J. Lehtinen, and A. Laaksonen, Atmos. Chem. Phys. **6**, 787 (2006).
[2] M. Kulmala, L. Laakso, K. Lehtinen, I. Riipinen, M. Dal Maso, T. Anttila, V.-M. Kerminen, U. Hõrrak, M. Vana, and H. Tammet, Atmos. Chem. Phys. **4**, 2553 (2004).
[3] M. Volmer, *Kinetik der Phasenbildung* (Steinkopff, Dresden und Leipzig, 1939).
[4] M. Volmer and A. Weber, Z. Phys. Chem. **119**, 277 (1925).
[5] L. Farkas, Z. Phys. Chem. **125**, 236 (1927).
[6] R. Becker and W. Döring, Ann. Phys. **24**, 719 (1935).
[7] J. Zeldovich, Zh. Eksp. Teor. Fiz. **12**, 525 (1942).
[8] P. Wagner, D. Kaller, A. Vrtala, A. Lauri, M. Kulmala, and A. Laaksonen, Phys. Rev. E **67**, 021605 (2003).
[9] N. Fletcher, J. Atmos. Sci. **26**, 1266 (1969).
[10] P. Hamill, C. S. Kiang, and R. D. Cadle, J. Atmos. Sci. **34**, 150 (1977).
[11] B. Z. Gorbunov, N. A. Kakutkina, and K. P. Koutzenogii, J. Appl. Meteorol. **19**, 71 (1980).
[12] B. Z. Gorbunov and N. A. Kakutkina, J. Aerosol Sci. **13**, 21 (1982).
[13] P. Hamill, R. P. Turco, C. S. Kiang, O. B. Toon, and R. C. Whitten, J. Aerosol Sci. **13**, 561 (1982).
[14] M. Lazaridis, M. Kulmala, and A. Laaksonen, J. Aerosol Sci. **22**, 823 (1991).
[15] M. Lazaridis, M. Kulmala, and B. Z. Gorbunov, J. Aerosol Sci. **23**, 457 (1992).
[16] D. Petersen, R. Ortner, A. Vrtala, A. Laaksonen, M. Kulmala, and P. E. Wagner, J. Aerosol Sci. **30**, S35 (1999).
[17] D. Petersen, R. Ortner, A. Vrtala, P. E. Wagner, M. Kulmala, and A. Laaksonen, Phys. Rev. Lett. **87**, 225703 (2001).
[18] H. Korhonen, I. Napari, C. Timmreck, H. Vehkamäki, L. Pirjola, K. E. J. Lehtinen, A. Lauri, and M. Kulmala, J. Geophys. Res. **108**, 4546 (2003).
[19] D. W. Lee, P. K. Hopke, D. H. Rasmussen, H. C. Wang, and R. Mavliev, J. Phys. Chem. B **107**, 13813 (2003).
[20] A. Määttänen, H. Vehkamäki, A. Lauri, S. Merikallio, J. Kauhanen, H. Savijärvi, and M. Kulmala, J. Geophys. Res. **110**, E02002 (2005).
[21] X. C. Zeng and D. W. Oxtoby, J. Chem. Phys. **95**, 5940 (1991).
[22] A. Laaksonen and D. W. Oxtoby, J. Chem. Phys. **102**, 5803 (1995).
[23] A. Laaksonen, J. Chem. Phys. **106**, 7268 (1997).
[24] V. Talanquer and D. W. Oxtoby, J. Chem. Phys. **106**, 3673 (1997).
[25] I. Napari and A. Laaksonen, J. Chem. Phys. **111**, 5485 (1999).
[26] J. Rowlinson and B. Widom, *Molecular Theory of Capillarity* (Clarendon, Oxford, 1989).
[27] K. Yasuoka and M. Matsumoto, J. Chem. Phys. **109**, 8451 (1998).
[28] K. Yasuoka and M. Matsumoto, J. Chem. Phys. **109**, 8463 (1998).
[29] K. Yasuoka, G. T. Gao, and X. C. Zeng, J. Chem. Phys. **112**, 4279 (2000).
[30] K. Laasonen, S. Wonczak, R. Strey, and A. Laaksonen, J. Chem. Phys. **113**, 9741 (2000).
[31] K. T. Kholmurodov, K. Yasuoka, and X. C. Zeng, J. Chem. Phys. **114**, 9578 (2001).
[32] S. Toxvaerd, J. Chem. Phys. **115**, 8913 (2001).
[33] P. Krasnochtchekov and R. S. Averback, J. Chem. Phys. **122**, 044319 (2005).
[34] J. K. Lee, J. A. Barker, and F. F. Abraham, J. Chem. Phys. **58**, 3166 (1973).
[35] N. G. Garcia and J. M. Soler Torroja, Phys. Rev. Lett. **47**, 186 (1981).
[36] P. R. ten Wolde and D. Frenkel, J. Chem. Phys. **109**, 9901 (1998).
[37] P. R. ten Wolde, M. J. Ruiz-Montero, and D. Frenkel, J. Chem. Phys. **110**, 1591 (1999).
[38] K. Oh and X. Zeng, J. Chem. Phys. **110**, 4471 (1999).
[39] B. N. Hale, Aust. J. Phys. **49**, 425 (1996).
[40] H. Vehkamäki and I. J. Ford, J. Chem. Phys. **112**, 4193 (2000).
[41] B. Chen, J. I. Siepmann, K. J. Oh, and M. L. Klein, J. Chem. Phys. **115**, 10903 (2001).
[42] R. A. Zahoransky, J. Höschele, and J. Steinwandel, J. Chem. Phys. **110**, 8842 (1999).
[43] B. J. C. Wu, P. P. Wegener, and G. D. Stein, J. Chem. Phys. **69**, 1776 (1978).
[44] T. Pierce, P. M. Sherman, and D. D. McBride, Astronaut. Acta **16**, 1 (1971).
[45] J. W. Lewis and W. D. Williams, National Technical Information Service Technical Report No. AD-782445, 1974 (unpublished).
[46] M. W. Matthew and J. Steinwandel, J. Aerosol Sci. **14**, 755 (1983).
[47] J. Steinwandel and T. Buchholz, Aerosol Sci. Technol. **3**, 71 (1984).
[48] G. D. Stein, National Technical Information Service Technical Report No. AD-A007357/7GI, 1974 (unpublished).
[49] A. Fladerer and R. Strey, J. Chem. Phys. **124**, 164710 (2006).
[50] J. Wölk and R. Strey, J. Phys. Chem. B **105**, 11683 (2001).
[51] J. Merikanto, H. Vehkamäki, and E. Zapadinsky, J. Chem. Phys. **121**, 914 (2004).
[52] B. N. Hale and D. J. DiMattio, J. Phys. Chem. B **108**, 19780 (2004).
[53] E. Blaisten-Barojas, I. L. Garzn, and M. Avalos-Borja, Phys. Rev. B **36**, 8447 (1987).
[54] M. A. Strozak, G. E. Lopez, and D. L. Freeman, J. Chem. Phys. **97**, 4445 (1992).
[55] N. Y. Matos and G. E. Lopez, J. Chem. Phys. **109**, 1141 (1998).
[56] I. Paci, I. Szleifer, and M. A. Ratner, J. Phys. Chem. B **109**, 12935 (2005).
[57] R. C. Ward, B. N. Hale, and S. Terrazas, J. Chem. Phys. **78**, 420 (1983).
[58] E. Zapadinsky, B. Gorbunov, V. Voloshin, and M. Kulmala, J. Colloid Interface Sci. **166**, 286 (1994).
[59] E. Zapadinsky and M. Kulmala, J. Chem. Phys. **102**, 6858 (1995).
[60] D. R. Nutt and A. J. Stone, Langmuir **20**, 8715 (2004).
[61] E. Zapadinsky, A. Lauri, and M. Kulmala, J. Chem. Phys. **122**, 114709 (2005).
[62] N. H. Fletcher, *The Physics of Rainclouds* (Cambridge University Press, Cambridge, 1962).
[63] H. Vehkamäki, *Classical Nucleation Theory in Multicomponent Systems* (Springer, Berlin, 2006).
[64] B. N. Hale and R. Ward, J. Stat. Phys. **28**, 487 (1982).
[65] I. Kusaka, Z.-G. Wang, and J. H. Seinfeld, J. Chem. Phys. **108**, 3416 (1998).
[66] F. F. Abraham, *Homogeneous Nucleation Theory* (Academic, New York, 1974).
[67] A. Bijl, Ph.D. thesis, University of Leiden, 1938.
[68] W. Band, J. Chem. Phys. **7**, 324 (1939).
[69] W. Band, J. Chem. Phys. **7**, 927 (1939).
[70] J. Frenkel, J. Chem. Phys. **7**, 538 (1939).
[71] J. Frenkel, J. Chem. Phys. **7**, 200 (1939).
[72] K. J. Oh and X. C. Zeng, J. Chem. Phys. **112**, 294 (2000).
[73] B. N. Hale, in *Proceedings of the 16th International Conference on Nucleation and Atmospheric Aerosols*, edited by M. Kasahara and M. Kulmala (Kyoto University Press, Kyoto, 2004), pp. 3–14.
[74] A. Lauri, J. Merikanto, E. Zapadinsky, and H. Vehkamäki, Atmos. Res. (in press).
[75] H. R. Pruppacher and J. D. Klett, *Microphysics of Clouds and Precipitation* (Kluwer Academic, Norwell, MA, 1997).
[76] C. H. Bennett, J. Comput. Phys. **22**, 245 (1976).
[77] S. Maruyama, T. Kimura, and M.-C. Lu, Therm. Sci. Eng. **10**, 23 (2002).
[78] N. Metropolis, A. W. Rosenbluth, M. N. Rosenbluth, A. H. Teller, and E. Teller, J. Chem. Phys. **21**, 1087 (1953).
[79] F. H. Stillinger, J. Chem. Phys. **38**, 1486 (1963).
[80] D. Frenkel and B. Smit, *Understanding Molecular Simulation*, 2nd ed. (Academic, New York, 2002).
[81] S. M. Thompson, K. E. Gubbins, J. P. R. B. Walton, R. A. R. Chantry, and J. S. Rawlinson, J. Chem. Phys. **81**, 530 (1984).
[82] A. Trokhymchuk and J. Alejandre, J. Chem. Phys. **111**, 8510 (1999).
[83] W. Wagner, Cryogenics **13**, 470 (1973).
[84] M. E. Fisher, Physics **3**, 255 (1967).
[85] A. Dillmann and G. E. A. Meier, J. Chem. Phys. **94**, 3872 (1991).
[86] F. B. Sprow and J. M. Prausnitz, Trans. Faraday Soc. **62**, 1105 (1966).